15C.7 Cyclone Fences around Tropical Cyclone Humberto (2001)

Gary M. Barnes and Klaus P. Dolling

University of Hawaii

1. Introduction

Do the horizontal mass and energy fluxes feeding the inner core (radius< 75 km) of a tropical cyclone (TC) affect the intensity of the TC? It has been established that the low-level inflow to a TC acquires energy from the sea, transports high angular momentum inward and eventually becomes the primary source for the main updrafts of the eyewall. This inflow is also where the equivalent potential energy (θ_e) increases substantially; that increase causes the TC to deepen (Malkus and Riehl (1960), Emanuel (1986), and Betts and Simpson (1987)).

The relationship between θ_e and TC intensification does not explicitly incorporate other eyewall characteristics such as its width, height, azimuthal completeness, mean rain rate, number of convective cells, updraft size, magnitude, and inflow depth. These variables likely have a relationship with the amount and rate of mass and water vapor processed by the eyewall.

Corresponding author: G. M. Barnes
Department of Meteorology, University of Hawaii
2525 Correa Road, Honolulu, Hawaii 96822
gbarnes@hawaii.edu

Latent heat release in the eyewall (e.g., Adler and Rodgers 1977, Rodgers and Adler 1981, Marks 1985, Cerveny and Newman 2000, Sitkowski and Barnes 2009), which is related to the horizontal moisture flux to the eyewall, has a positive correlation with TC intensity for most but not all of the aforementioned studies.

The inflow that supplies the eyewall can be highly asymmetric despite the strong rotational nature of the inner core. This asymmetry of the inflow has been related to TC motion, the vertical shear of the horizontal wind, and nearness to land. Shapiro (1983) used a slab boundary layer model of a symmetric translating vortex to show convergence in a broad arc on the leading edge of the eyewall. Vertical shear of the horizontal wind through the troposphere (hereafter vertical wind shear, VWS) has been correlated with asymmetries in the reflectivity field (Black et al. 2002), lightning distribution (Molinari et al. 1999) and presumably, the low-level inflow to the hurricane core. Eastin et al. (2005) found the most buoyant and vigorous convective updrafts down shear and to the left of the VWS vector for the eyewalls of Guillermo (1997) and Georges (1998). Numerical simulations (Bender 1997, Frank and Ritchie 1999, Braun 2002, Wu et al. 2006, Braun et

al. 2006) showed maximum lifting down shear and to the left of the VWS vector. Corboserio and Molinari (2003) have noted that the VWS and motion vectors are frequently related with the VWS vector about 70 degrees clockwise from the motion vector.

The third factor that has been proposed to impact the inflow pattern is the asymmetric friction caused by the presence of land near the hurricane. Kepert (2006) examined Mitch (1998) which was nearing Honduras and diagnosed inflows that were asymmetric with the maximum found to the left of the TC motion vector (looking in the direction of the vector) verifying the numerical simulations by Kepert and Wang (2001). Another TC that had its maximum inflow on the left rear quadrant was Bonnie (1998); this TC was observed just prior to landfall (Schneider and Barnes 2005) lending credence to the argument that the enhanced friction over land altered the force balance causing the inflow asymmetry.

During September of 2001 NOAA and NASA aircraft sampled Tropical Cyclone Humberto while participating in CAMEX-IV. Over 200 hundred Global Positioning System dropwindsondes (GPS sondes) were deployed within 150 km of the circulation center over 3 consecutive days. These sondes provide an opportunity to examine the low-level inflow to Humberto (2001) as it evolved from a tropical storm with a central pressure of 1000 hPa on September 22nd to 983 hPa on the 23rd, then weakened to 992 hPa by the 24th.

Our purpose is to describe the evolving character of the inflow over these 3 days. Specifically we will create azimuth-height (φ-z) surfaces that extend from the sea surface to 3 km altitude for the .25° and .50° latitude rings around the circulation center. We will identify the magnitude, depth and azimuthal extent of the inflow on these surfaces. The mass and energy fluxes through these azimuth-height surfaces ("cyclone fences") will be estimated. The motion and VWS vectors will be determined for each day to ascertain how these factors are correlated with the inflow pattern. The two ring choices (.25° and .50°) are a function of what was observed with radar and the sonde distribution. Our radar analysis shows that the inner ring is dominated by stratiform rain on the 22nd, followed by a partial eyewall near that inner .25° radius on the 23rd and then a reformation of the convection beyond that ring on the 24th. There is always convective activity within .50° of the center for the 3 days. Sonde distribution is such that we cannot adequately determine the flow for a ring much smaller than .25°.

2. Data and Methodology

We use the Global Positioning System dropwindsondes (GPS sondes) which have a 2 Hz sampling rate and realize ~7 m vertical resolution in the lower troposphere. Typical errors for pressure, temperature (T), and relative humidity (RH) are 1.0 hPa, 0.2 °C, and <5%, respectively (Hock and Franklin 1999).

On the 22nd of September ~95% of the 30 GPS sondes recorded data successfully. Ninety-six GPS sondes were deployed on the 23rd and 102 were dropped on the 24th. Figure 1a, b shows the locations of the sondes relative to the TC center on the 22nd and the 23rd; the 24th pattern is essentially identical to the prior day.

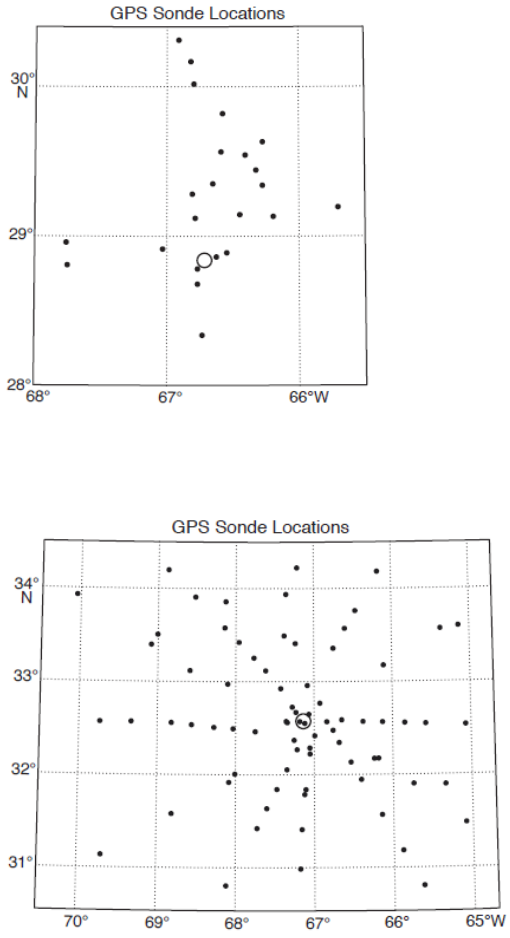

Fig. 1. (top) Location of the GPS sondes on the (a) 22nd of September and (bottom) 23rd of September relative to the circulation center. Drop locations for the 24th are almost in the same location relative to the circulation center. Center of the TC is the larger open circle.

The analysis scheme includes the determination of the circulation center using the technique of Willoughby and Chelmow (1982). Sonde location relative to the circulation center for every moment of its descent is determined so storm relative flows can be estimated. Gaps in the data less than 300 m thick were linearly filled and these data were standardized to common altitudes. Finally a cubic spline was used to create x-y maps from the three-dimensional matrix. More details of the analysis scheme can be found in Dolling and Barnes (2012a, b). Humberto's minimum sea-level pressures varied only a few hPa during the 3 to 4 hours of any mission so we will assume an approximately steady-state for each day. Beven et al. (2003) review the life cycle of Humberto (2001).

3. Preliminary Results

a. TC intensity, motion and environmental shear

Early on September 22nd, Humberto was a tropical depression with a minimum central pressure of 1010 hPa and was located in the Atlantic basin near 29^0 N and 66^0 W. The movement was to the north-northwest at approximately 4 m s^{-1} (Fig. 2). Humberto continued moving to the north and eventually recurved to the northeast, increasing speed to 7 m s^{-1} by the time of the final missions on the 24th. When the first GPS sondes were jettisoned, late on the 22nd, Humberto's minimum central pressure was 1000 hPa and it had attained tropical storm intensity. Twenty four hours later on the 23rd, it deepened to 983 hPa. Humberto weakened to 992 hPa by the mission on the

24th. Fig. 2 also reveals the deep layer VWS vector as determined from SHIPS (DeMaria and Kaplan 1994, DeMaria et al. 2005). The shear vector is 11 m s^{-1} on the last two days.

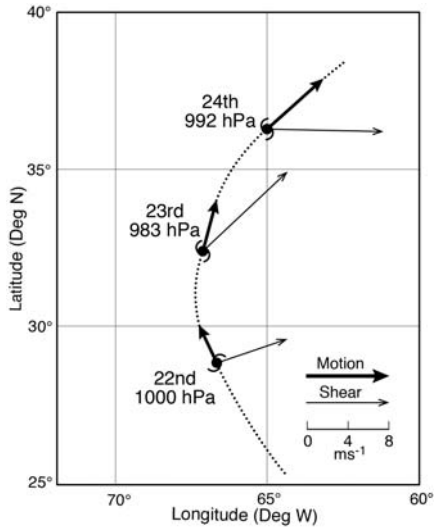

Fig. 2. Track of Humberto (2001) with motion (dark arrow) and deep layer vertical wind shear (thin arrow) vectors as a function of latitude and longitude. Date and mean sea-level pressure shown for each location when the TC was sampled by the aircraft.

b. Reflectivity patterns for each day

During the mission on the 22nd Humberto's rain field is dominated by an arc of convective clouds about 50 km from the circulation center extending from the NW through the SE quadrants (Fig. 3a). The tops of the cells in this arc reach to 15-16 km altitude. Closer to the circulation center there are two cells in their early stages of development and over the center there is stratiform rain. The echoes in the band trailing to the south are shallower with tops reaching to 6-8 km. Note that the majority of the echoes with reflectivities greater than 40 dBZ reside in the .25° to .5° latitude annulus shown in the figure.

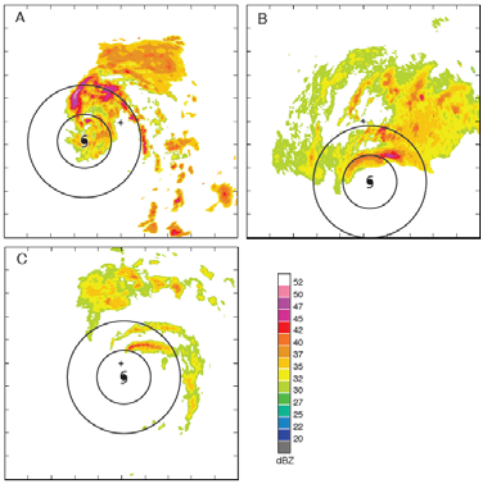

Fig. 3. Reflectivity fields from the NOAA WP-3D for (a) 1900 on the 22nd, (b) 2037 on the 23rd, and (c) 2251 on the 24th of September. Reflectivities below 30 dBZ have been excised to remove extensive sea-clutter; scale is 240 x 240 km. Aircraft position is the cross and storm center is the hurricane symbol. Range rings are .25 and .50 degrees latitude from the TC center.

From the 22nd to the 23rd Humberto deepens 17 hPa. A crescent shaped eyewall with reflectivity exceeding 45 dBZ is 25-30 km N of the circulation center (Fig. 3b). Most of the other convective cells within 100 km of the center are in the N quadrant. The eye is now clear of any stratiform rain. The eyewall maintains an elliptical shape throughout the mission based on examination of other lower fuselage radar views.

From the 23rd to the 24th Humberto fills 9 hPa. The eyewall is in the shape of a flattened arc to the NNE of the circulation center and now lies outside of .25° radius. The key point is that there is very little convective activity within .25° of the center

on the first and third days while on the second day the eyewall is just at this distance and remains a steady feature throughout the mission on that day.

c. Radial wind component on φ-z surfaces

We show the azimuth-height (φ-z) surface for the .25° ring for each of the 3 days of sampling. The ring or "cyclone fence" should be viewed technically as a swath given that the sondes that contributed to the field vary by 5 to10 km on either side of a chosen radius.

The radial winds (Vr) for the .25° (Fig. 4a-c) reveal the following structure highlights that appear to be independent of either deepening or filling:

(1) all 3 days clearly manifest a wave number one pattern,

(2) the center of the inflow channel rotates anticyclonically from N to E over the 3 days,

(3) the center of the outflow channel remains in the SW octant over the 3 days,

Based on the aforementioned work that identified a relationship between the motion or VWS vector and the location of either convergence, inflow, updraft location or reflectivity maxima one would have predicted that the inflow would lie in the N through E quadrants, which it does (Fig. 2). The strongest inflow (Vr < -10 m s^{-1}) is where the expected forcing from the motion and the VWS are collocated.

From the 22nd to the 23rd the TC deepens 17 hPa. The major changes in the radial flow include:

(1) expansion of the inflow by ~60°,

(2) an increase of several m s^{-1} in the heart of the inflow,

(3) a deepening of the inflow, and

(4) a large increase (>10 m s^{-1}) in the magnitude of the outflow.

From the 23rd to the 24th the TC filled 9 hPa and the following were noted:

(1) azimuthal extent of the inflow and its speed remained essentially constant,

(2) depth of the inflow decreased, and

(3) speed of the outflow decreased markedly.

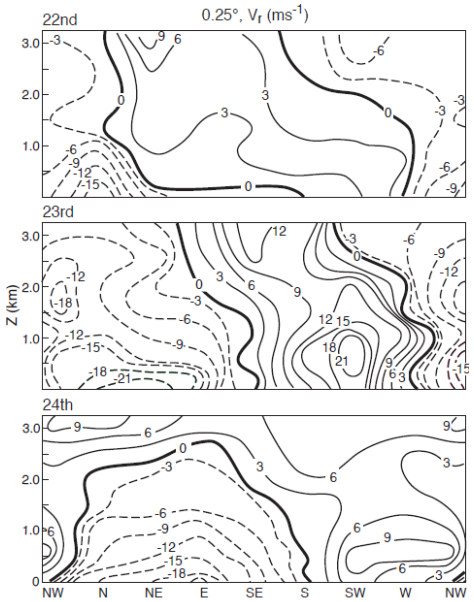

Fig. 4. The radial wind component in 3 m s^{-1} contours for the .25° φ-z surface from the sea-surface to 3 km altitude for the 22nd (top panel), the 23rd (middle panel) and the 24th (bottom panel). Negative sign depicts inflow.

d. Mass flux through .50 and .25 degree circles

The radial wind fields shown in Fig. 4 and for the .50° ring (not shown) can be used to produce estimates of the horizontal mass flux from the sea surface to 3 km altitude. Here we have calculated the mean

radial wind for each octant, estimated the density for 500 m layer increments using the thermodynamic data along the φ-z surface and multiplied these by the area for each octant for a given radius. Mass flux can be used to highlight the relative importance of each layer that either feeds or extracts air from a chosen volume and it can be related to divergence and the number of convective elements that exist within a given region.

The total azimuthal mass flux for the .50° and the .25° radius circles from the sea to 3 km for each day appear in Fig. 5. Three volumes are discussed: that within .50°, the annulus between .50° and .25°, and that circumscribed by the .25° radius circle. On the 22nd the total mass inflow through the .50° circle was 2.7 x 10^9 kg s^{-1} and the outflow was -2.0 x 10^9 kg s^{-1} (Fig. 5 top left panel) resulting in a net upward flux of 0.7 x 10^9 kg s^{-1} (Fig. 5 top right panel). The approximate center of the mass flux, both in and out, for the 3 km layer is depicted by where the value is placed on the circle in Fig. 5. For the 22nd the inward mass flux was N of the center and the outflow was to the SSE and S. For the volume encompassed by the .25° circle there was a net loss of mass – the inner volume was dominated by subsidence and was under the influence of stratiform rain during most of the data gathering on the 22nd. The annulus defined by the two circles had a net flux that is positive (0.8 x 10^9 kg s^{-1}, Fig. 5, top right panel). This annulus is where the main arc of convection was present (Fig. 3a) and thus where we would expect to see a net upward flux.

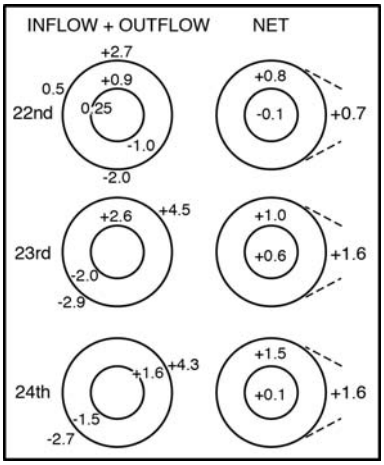

Fig. 5. In the 3 left panels the horizontal mass flux in (positive) and out (negative) for the 3 days for .25° and .5° φ-z surfaces are shown. Units are x 10^9 kg s^{-1}. The location of the value depicts the center of the inflow or outflow through the 3 km height of the φ-z surface. The 3 right panels depict the net or vertical mass flux for three volumes for each day: the number to the right is for the entire .5°, the number in the ring is for the annulus between .5° and .25°, and the number in the center is for the volume circumscribed by the .25° ring. Negative is net downward, positive is net upward mass flux in units of x 10^9 kg s^{-1}.

As the TC intensified on the 23rd the mass flux into the φ-z surface at .50° increased to 4.5 x 10^9 kg s^{-1} and the outward flux increased to -2.9 x 10^9 kg s^{-1} (Fig. 5 middle panels); the net upward flux of 1.6 x 10^9 kg s^{-1} is an increase of 2.3x compared to the previous day. The inward and net fluxes for the inner .25° both increased on the 23rd; this change to a large net upward flux on the 23rd (+.6 x 10^9 kg s^{-1}) during intensification was correlated with the development of the eyewall that resided just within the .25°

radial distance. The center of the inflow, density weighted from the sea surface to 3 km shifted toward the NE and the outflow was located to the SW. The net mass flux in the annulus defined by the two rings was slightly larger than the day before (1.0×10^9 kg s^{-1}). Figure 3b reveals that this annulus continued to be the location for a band of deep convection to the N and NE.

From the 23rd to the 24th the TC filled 9 hPa and the eyewall became disorganized as it reformed beyond .25° (Fig. 3c). The mass flux in and out of the .50° circle changed little from the prior day. For the .25° volume the net mass flux was barley positive and less than 20% of what was estimated on the 23rd; this reduction coincided with the disappearance of deep convection for the 24th within the inner circle. The annulus between the two rings had a net upward flux of 1.5×10^9 kg s^{-1}; this large value corresponds to both the inner bands and the reforming eyewall residing in this region.

The amount of inflow into the .50° ring exceeds that entering the .25° ring for all 3 days. Only 33% of the inflow that was estimated at .5° reached the inner ring on the 22nd. This percentage increased to 58% on the 23rd when the TC was at its most intense; it decreased to 37% on the 24th. There are obviously significant losses as air ascends in the annulus defined by the .50° and .25° rings. More inflow reached the smaller radius when the TC achieved its' greatest intensity on the 23rd.

4. Conclusions

We have used GPS sondes deployed over 3 consecutive days to create azimuth-height surfaces, our so-called cyclone fences, which extend from the sea to 3 km altitude for two rings located .25° and .5° latitude from the center of Humberto (2001). The radial flow normal to these two φ-z surfaces reveals that a wave number one pattern is maintained as Humberto deepens 17 hPa from the 1st to the 2nd day then later fills 9 hPa by the 3rd day. The location of the inflow adjusts to remain aligned with the motion vector and down shear of the VWS vector. Both vectors favor inflow in the same quadrants which may be contributing to the marked asymmetry of the TC. During deepening the inflow never becomes a complete ring, instead a strong outflow is seen in the low levels even as the TC increases in intensity.

Only the net mass flux for the .25° azimuth-height surface is positively correlated with intensity. This flux is, as expected, associated with the reflectivity fields found within the .25° ring. TC intensity does not respond to net mass flux for the .5° ring. The large net upward flux within 50 - 60 km of the circulation center support rainbands that apparently do not contribute to the strength of the warm core. Why are these bands, only 50-60 km from the circulation center, ineffective at producing a warm core? We suspect that the strong VWS is a clue. Arcs of convection that are far from the circulation center are susceptible to environmental air eroding the

warm core. A few cumulonimbi at smaller radii can cover a greater azimuthal extent and their outflows may counter erosion of the warm core by environmental flows. The presentation will cover both rings as well as energy flux.

Acknowledgements: We deeply appreciate the effort made by NOAA- Aircraft Operations Center, The Hurricane Research Division of the NOAA- Atlantic Oceanographic and Meteorological Laboratory and the NASA scientists during the 2001 Hurricane season. This research is supported by NSF Award AGS-1042680.

5. References

Adler, R. F., and E. B. Rodgers, 1977: Satellite-observed latent heat release in a tropical cyclone. *Mon. Wea. Rev.*, **105**, 956-963.

Bender, M. A., 1997: The effect of relative flow on the asymmetric structure of the interior of hurricanes. *J. Atmos. Sci.*, **54,** 703–724.

Betts, A. K. and J. Simpson, 1987: Thermodynamic budget diagrams for the hurricane subcloud layer. *J. Atmos. Sci.*, **44**, 842-849.

Beven, J.L., S. R. Stewart, M. B. Lawrence, L. A. Avila, J. L. Franklin, and R. J. Pasch, 2003: Annual summary – Atlantic season of 2001. *Mon. Wea. Rev.*, **131**, 1454-1484.

Black, M.L., J.F. Gamache, F.D. Marks Jr., C.E. Samsury, and H.E. Willoughby, 2002: Eastern Pacific Hurricanes Jimena of 1991 and Olivia of 1994: The Effect of Vertical Shear on Structure and Intensity. *Mon. Wea. Rev.*, **130**, 2291-2312.

Braun, S. A., 2002: A cloud-resolving simulation of Hurricane Bob (1991): Storm structure and eyewall buoyancy. *Mon. Wea. Rev.*, **130**, 1573-1592.

_____, M. T. Montgomery and Z. Pu, 2006: High-resolution simulation of Hurricane Bonnie (1998). Part I: The organization of eyewall vertical motion. *J. Atmos. Sci.*, **63**, 19-42.

Cerveny, R. S., and L. E. Newman, 2000: Climatological relationships between tropical cyclones and rainfall. *Mon. Wea. Rev.*, **128**, 3329-3336.

Corbosiero, K. L., and J. Molinari, 2003: The Relationship between Storm Motion, Vertical Wind Shear, and Convective Asymmetries. *J. Atmos. Sci.*, **60**, 366-376.

DeMaria, M., M. Mainelli, L. K. Shay, J. A. Knaff, and J. Kaplan, 2005: further improvements to the statistical hurricane intensity prediction scheme (SHIPS). *Wea. Forecasting*, **20**, 531-543.

_____, and J. Kaplan, 1994: A Statistical Hurricane Intensity Prediction Scheme (SHIPS) for the Atlantic basin. *Wea. Forecasting*, **9**, 209-220.

Dolling, K. P., and G. M. Barnes, 2012a: The creation of a high equivalent potential temperature reservoir in Tropical Storm Humberto (2001) and its' possible role in storm deepening. *Mon. Wea. Rev.,* **140**, 492-505.

_____, and G. M. Barnes, 2012b: Warm-core formation in Tropical Storm Humberto (2001). *Mon. Wea. Rev.,* **140**, 1177-1190.

Eastin, M.D., W. M. Gray and P. G. Black, 2005: Buoyancy of convective vertical motions in the inner core of intense hurricanes. Part II: Case Studies. *Mon. Wea. Rev.*, **133**, 209- 227.

Emanuel, K.A., 1986: An air-sea interaction theory for tropical cyclones. Part I: Steady-state maintenance. *J. Atmos. Sci.*, **43**, 585–605.

Frank, W.M., and E.A. Ritchie, 1999: Effects of Environmental Flow upon Tropical Cyclone Structure. *Mon. Wea. Rev.*, **127**, 2044-2061.

Hock, T.F., and J.L. Franklin, 1999: The NCAR GPS dropwindsonde. *Bull. Amer. Meteor. Soc.*, **80**, 407-420.

Kepert, J.D., 2006: Observed Boundary Layer Wind Structure and balance in the Hurricane Core. Part II: Hurricane Mitch. *J. Atmos. Sci.*, **63**, 2194-2211.

_____, and Y. Wang, 2001: The dynamics of boundary layer jets within the tropical cyclone core. Part II: Nonlinear enhancement. *J. Atmos. Sci.*, **58**, 2485-2501.

Malkus, J. S. and H. Riehl, 1960: On the dynamics and energy transformations in steady-state hurricanes. *Tellus*, **12**, 1-20.

Marks, F.D., Jr., 1985: Evolution of the structure of precipitation in Hurricane Allen. *Mon. Wea. Rev.*, **113**, 909-930.

_____, R. A. Houze, and J. F. Gamache, 1992: Dual-aircraft investigation of the inner core of Hurricane Norbert. Part I: Kinematic structure. *J. Atmos. Sci.*, **49**, 919-942.

Molinari, J., P. K. Moore, and V. P. Idone, 1999: Convective structure of hurricanes as revealed by lightning locations. *Mon. Wea. Rev.*, **127**, 520-534.

Rodgers, E. B., R. F. Adler, 1981: Tropical cyclone rainfall characteristics as determined from satellite passive microwave radiometer. *Mon. Wea. Rev.,* **109**, 506-521.

Schneider, R., and G. M. Barnes, 2005: Low-level kinematic, thermodynamic, and reflectivity fields associated with Hurricane Bonnie (1998) at landfall. *Mon. Wea. Rev.*, **133**, 3243-3259.

Shapiro, L.J., 1983: The asymmetric boundary layer flow under a translating hurricane. *J. Atmos. Sci.*, **40**, 1984-1998.

Sitkowski, M., and G.M. Barnes, 2009: Low-level thermodynamic, kinematic, and reflectivity fields of Hurricane Guillermo (1997) during Rapid Intensification. *Mon. Wea. Rev.*, **137**, 645-663.

Willoughby, H. E., and M. B. Chelmow, 1982: Objective determination of hurricane tracks from aircraft observations. *Mon. Wea. Rev.*, **110**, 1298-1305.

Wu, L., S. A. Braun, J. Halverson, and G. Heymsfield, 2006: A numerical study of Hurricane Erin (2001). Part I: Model verification and storm evolution. *J. Atmos. Sci.*, **63**, 65- 86.